Wearable and fully printed microfluidic nanosensor for sweat rate, conductivity, and copper detection for diseases prevention

*Qiuyue Yang[a,b†], Giulio Rosati[a†], Vernalyn Abarintos[a,c], Miguel Angel Aroca[d,e], Johan Faccelo Osma[d], Arben Merkoçi[a,f]**

[a] Catalan Institute of Nanoscience and Nanotechnology (ICN2), Edifici ICN2, Campus UAB, 08193 Bellaterra, Barcelona, Spain

[b] Universitat Autònoma de Barcelona, Department of Material Science, Campus de la UAB, Plaça Cívica, 08193 Bellaterra, Barcelona.

[c] Universitat Autònoma de Barcelona, Department of Biotechnology, Campus de la UAB, Plaça Cívica, 08193 Bellaterra, Barcelona.

[d] Department of Electrical and Electronic Engineering, Universidad de los Andes, Cra 1 Nº 18A – 12, 111711, Bogotá, Colombia

[e] Office of Information and Communication Technologies. Government of Cesar. Calle 16 # 12 - 120 Alfonso López Michelsen Building, Valledupar, Colombia

[f] Catalan Institution for Research and Advanced Studies (ICREA), Passeig de Lluís Companys, 23, 08010 Barcelona, Spain

[†]These authors equally contributed to this publication

*Corresponding author. Nanobioelectronics & Biosensors Group, Institut Català de Nanociància i Nanotecnologia (ICN2), CSIC and The Barcelona Institute of Science and Technology (BIST), Campus UAB, 08193, Bellaterra, Barcelona, Spain. E-mail address: arben.merkoci@icn2.cat (A. Merkoçi).

Abstract

Wearables are becoming pervasive in our society but still mainly based on physical sensors, with just few optical and electrochemical exceptions. Sweat, between other body fluids, is easily and non-invasively accessible, abundant, and relatively poor of interfering species. The biomarkers of interest in sweat space from ions and small molecules to whole organisms. Heavy metals have a relevant role, and copper in particular has been found being a biomarker of several diseases and pathological conditions such as Wilson's disease and liver cirrhosis. Nevertheless, several issues, such as sampling conditions, sweat rate normalization, reliable continuous monitoring, and typically expensive fabrication methods, characterize sweat analysis with wearables. Herein, we propose a fully printed wearable microfluidic nanosensor with an integrated wireless smartphone-based readout. Our system can easily be applied on the skin and actively stimulate perspiration, normalizing the heavy metals concentration with respect to the volume of the sample and the sweat rate. The system has a limit of detection of 396 ppb, a linear range up to 2500 ppb and a sensitivity of 2.3 nA/ppb.

Keywords: Sweat analysis, nanofunctional inks; heavy metals; wearables; flexible electronics; smartphone readout.

1. Introduction

Wearable sensors and biosensors, most often referred simply as wearables are already devices of common use in our society. The main applications currently covered by these devices are wellbeing and sport, with physical sensors based on gyroscopes and accelerometers and optical sensors for the measurement of the heart rate. Despite these sensing methods are relatively basic with respect to the ones available in scientific literature, these wearables have clearly showed the relevance of continuous wireless/remote monitoring, big data analysis, and proper results visualization. Another very impacting application, not

second in importance are continuous glucose monitoring (CGM) systems, which are measuring the glucose concentration under the skin (blood or interstitial fluid) in real-time and continuously for up to 10 days. Lactate measuring devices using a similar approach are attracting interest as well, mainly for sport applications.

In the last years, the number of scientific publications on wearables are increasing exponentially. These are addressing several open issues, such as the resilience of wearables for long periods in contact with the body fluids, smart solutions for the power supply of the devices and for their wireless readout, and the detection of always new biomarkers to spread the use of these systems for multiple applications in healthcare and lately also for environmental applications. Recent developments have focused on electrochemical and optical biosensors, together with advances in the noninvasive monitoring of biomarkers including metabolites, bacteria and hormones (Kim et al. 2019). Advances in the miniaturization of flexible electronics, electrochemical biosensors, microfluidics, and artificial intelligence algorithms have led to wearable devices that can generate real-time medical data within the Internet of things (Yetisen et al, 2018). The potential of these systems is extremely high and their typologies and characteristics so variegated to entail and require very interdisciplinary efforts to be pursued and developed (Morales-Narvaez and Dincer, 2021).

All the wearables are composed by the same units: the sample collector, the sensor (integrating the eventual bioreceptor and the transducer), the readout system, and the data analysis and results displaying/transmission. However, their properties and characteristics vary mainly in relation with the type of sample to be analyzed. By definition, a wearable should target non-invasive sampling, thus the typically addressed samples are interstitial fluid, blood, tears, and sweat. The latter being the simplest in composition, abundant, and containing many biomarkers for pathologies and for the general wellbeing of the subject (Bariya et al., 2018). For these reasons, the wearables based on sweat have attracted relevant attention (Ghaffari et al., 2021; Mohan et al., 2020; Qiao et al., 2020; Xu et al., 2021; Bandodkar et al., 2019; Jo et al., 2021; Brothers et al., 2019; Chung et al., 2019).

Despite the low level of interference due to its simple composition and its relative abundancy, sweat has intrinsic issues related to its extraction (Liu et al., 2020). Sweat can be obtained both passively, thanks to an increased temperature or physical exercise, and actively, by using drugs or electrical currents (*i.e.* reverse iontophoresis - Bariya et al., 2018). However, the amount of sweat excreted for unit of time, *i.e.* the sweat rate, changes during the perspiration and affects the concentration of the biomarkers present in the sweat. The sweat rate itself can give valuable information about the health status, thus it has already been addressed by simple wearables, typically employing microfluidic channels (Salvo et al., 2010; Nyein et al., 2018). In addition to these issues, the concept of continuous monitoring is rarely met in reality. In fact, sweat wearables typically have a short duration or are designed for single use (Vaquer et al., 2020; Lee et al., 2020; Zhong et al. 2019; Vinoth et al., 2021). Despite many publications claims the real-time characteristics of the respective sensors, this concept does not correspond to the one of continuous monitoring. The few ones truly performing continuous detection are measuring only simple characteristics such as the pH or the ions content (Nyein et al., 2019; Anastasova et al., 2017).

Sweat conductivity alone is an interesting analyte, well known for the cystic fibrosis (CF) diagnosis as an alternative to the standard quantification of the Na^+ and/or Cl^- ions. CF is an inherited disorder that causes a failure of the innate airway defense mechanisms, and the damage of the digestive system and other organs in the body. It is normally accompanied by high concentration of salts in sweat, and the associated cut-off conductivity in sweat for the CF diagnosis is over 90 mM (Lezana et al., 2003).

Between the many biomarkers in serum and sweat, heavy metals (HMs) have an important role. Copper for example is involved in many pathological conditions. Imbalance in the copper/zinc ratio is suspected to be related to coronary heart disease (Klevay 1975), serum copper can be used as biomarker of rheumatoid arthritis (Youssef et al., 1983), Wilson's disease (Sunderman et al., 1974; Schaefer et al., 2008), and liver cirrhosis (Agarwal et al., 2017; Nangliya et al., 2015, Vierling 2008). Furthermore, copper and others heavy metals in sweat show important variations related to the physical exercise, heat

stress, and diet (Montain et al., 2007; Aruoma et al., 1988; Saraymen et al., 2004; Gutteridge et al., 1985; Saraymen et al., 2003; Tomasz et al., 2018; Siquier-Coll et al., 2020).

So far, only few biosensors have targeted copper and other heavy metals in sweat. In 1987 Stauber and Florence, showed how to use stripping voltammetry to perform copper detection in sweat (Stauber and Florence, 1987). In 2010, Souza et al. have showed the use of a gold microelectrode for the detection of copper in sweat (Souza et al., 2010). However, the presented system was not wearable but based on a standard three-electrodes electrochemical setup. Recently, Bagheri et al. proposed a sensor based on gold nanoparticles-decorated paper for the sensitive detection of copper in sweat and serum (Bagheri et al., 2021). This simple single-use system, based on screen-printing and wax printing on paper, proved to be very effective for copper determination, with limit of detection of 3 ppb, a linear range up to 400 ppb and recoveries between 93% and 101% in spiked sweat. Despite these very promising characteristics, this system is not wearable, cannot be used more than once, and needs a potentiostat to perform the quantification.

In this work, we propose an all-printed wearable system composed of an inkjet-printed microfluidic part for the active sampling thanks to reverse iontophoresis and able to measure the sweat volume/rate, a screen-printed carbon electrode (SPCE) for the copper electrochemical detection and its concentration normalization with the sweat rate, and finally a flexible wearable potentiostat transmitting the data wireless to a smartphone. The whole system is flexible and lightweight. It can be applied directly on the skin with a patterned biadhesive and managed remotely. Our low-cost fully printed system can be fabricated out of the cleanroom and even out of the lab, with simple printing and patterning techniques. The copper sensor showed a limit of detection of 396 ppb, a linear range up to 2500 ppb, a sensitivity of 2.3 nA/ppb, and resilience to interference tested in artificial sweat. Finally, the simple addition of a paper sponge in correspondence of the outlet makes possible the sweat extraction and evaporation from the microchannel, allowing the system reuse over time, pursuing the continuous monitoring concept.

2. Materials and Methods

2.1 Materials and apparatus

37% Hydrochloric acid (3203312.5L), standard heavy metal solutions (Cu, Zn, Cd, Ni, 1000ppm, AAS grade) were purchased from Sigma Aldrich. The potentiostat used for the characterizations was a Palmsens EmStatBlue. The software used for the HM detection was PStrace 5.8. The artificial sweat used for the system validation is composed of 0.1M NaCl, 0.1 wt% KCl, 0.1 wt% lactic acid, 0.1 wt% urea in acetate buffer (0.1M, pH=4.5) (Silva et al., 2020).

2.2 Fabrication of SPCEs

The SPCEs were fabricated using a DEK248 printer machine (DEK, Weymouth, UK). PET has been cleaned with deionized water and ethanol, then dried with nitrogen and pre-heated at 110°C for 30 min to evaporate solvents and prevent deformation in the following steps. The printing sequence on the prepared PET substrate and the used inks are the following: (1) Ag paste (C2180423D2 SILVER PASTE-349288, Sun Chemical) for conductive connections, (2) Ag/AgCl paste (Loctite EDAG AV458, Henkel) for the reference electrode, (3) carbon paste (C2030519P4 CARBON SENSOR PASTE-267508, Sun Chemical) for the working and counter electrodes, (4) and the insulating layer (D2070423P5 DIELECT PASTE GREY, Sun chemical). The inks were cured at 110 °C for 30 min in oven after every printing step (Yang et al., 2021).

2.3 Inkjet printing and passivation

All the silver nanoparticles (AgNPs) electrodes and contacts were inkjet-printed with Mitsubishi Paper Mills Silver Nano™ AgNP ink (NBSIJ-MU01) on Mitsubishi Paper Mills special substrate (NB-TP-3GU100) by an EPSON XP15000 printer. The devices were kept for 72 hours at room temperature before performing the following step in order to have a stable resistance of the electrodes. Then, a layer of wax (black color, Xerox Phaser 8850) has been printed in the area over and around the electrodes. The printed

wax and Ag device was kept at 95º for 20 seconds to partially melt the wax and allow its penetration in the substrate permeable coating structure. A second wax layer was printed and kept in the oven for 5 minutes to ensure a complete filling of the coating in the area of interest. (Rosati et al. 2021). The first set of parallel electrodes were designed with a finger width and a gap of 400 µm, and oriented perpendicularly with respect to the microchannel, crossing it completely thus having a length of 2 mm in contact with the solution. The second set of parallel electrodes were designed to be as long as the channel (30 mm) and parallel to it and with a gap of 200 µm.

2.4 Biadhesive laser cutting and microfluidic circuit assembling

OPP biadhesive A4 sheets (Tosingraf, Italy) were patterned by laser cutting (Rayjet 50™ CO_2 laser) to fabricate a fluidic channel (power: 6.9%, speed: 100%, number of passages: 4). The assembly of the microfluidic circuit has been done by applying the patterned bioadhesive over the inkjet printed substrate and closing the channel with the screen-printed device, flipped upside down, as can be seen on Figure 1(a). Just before assembling it, the inkjet-printed layer has been shortly treated (15 s) by atmospheric plasma to increase its hydrophilicity. Finally, the whole system was inserted in a laminator (Lamigator IQ, Renz, Germany) between two sheets of office paper to homogeneously compress it, secure spaces, and avoid leakage.

2.5 HM sensing and Electrochemical Impedance Spectroscopy (EIS) measurements

The HM ions detection was performed by Square Wave Anodic Stripping Voltammetry SWASV in three steps. First the ions deposition on the working electrode, then the equilibrium, and finally the stripping. During the deposition step, a constant negative potential of -0.66 V was applied to the working electrode for a period of 200 s, followed by an equilibrium period of 20 s. Finally, the potential was swept from -0.66 V to 0 V in square-wave pulses for the stripping step with a frequency of 25 Hz, an amplitude of 30 mV, and a potential step of 6 mV.

To avoid the formation of bubbles on the surface of the carbon materials, the screen-printed device was firstly rinse with artificial sweat for 10 min and nitrogen was used to blow the liquid inside the micro-chamber/channel. For the impedance measurements on the inkjet-printed electrodes, the fabricated devices were connected to a Metrohm AutoLab PGSTAT12 (FRA2) potentiostat, and the EIS measurements were performed in triplicate at 100 kHz, with 10 mVpp AC and 0 V DC.

3. Results and Discussion

3.1 Design and fabrication of the printed microfluidic device

The printed microfluidic device was designed and fabricated with three integrated sensors: a screen-printed carbon electrode (SPCE) for HM sensing, a conductivity nanosensor composed of interdigitated silver nanoparticles (AgNP) electrodes (perpendicular with respect to the microchannel), and a volume nanosensor consisting of two AgNP electrodes parallel to the microfluidic channel. (Figure 1(a))

With the help of the laser cut biadhesive tape, a microchamber and microchannel has been defined between the SPCE (and its PET substrate) and the wax printed pad. In this way, the sampled sweat can flow firstly through the chamber beneath the SPCE (HM microchamber), then through the conductivity nanosensor, and finally along the volume nanosensor microchannel. The conductivity nanosensor also generates the trigger signal for the HM sensing, ensuring the chamber has been completely filled. Once triggers, the SPCE performs a SWASV in the HM microchamber. During the HM measurement, the volume nanosensor changes its impedance depending on its coverage by sweat along the channel, giving an indirect measurement of the collected sweat volume and allowing the calculation of the sweat rate with real-time impedance measurements.

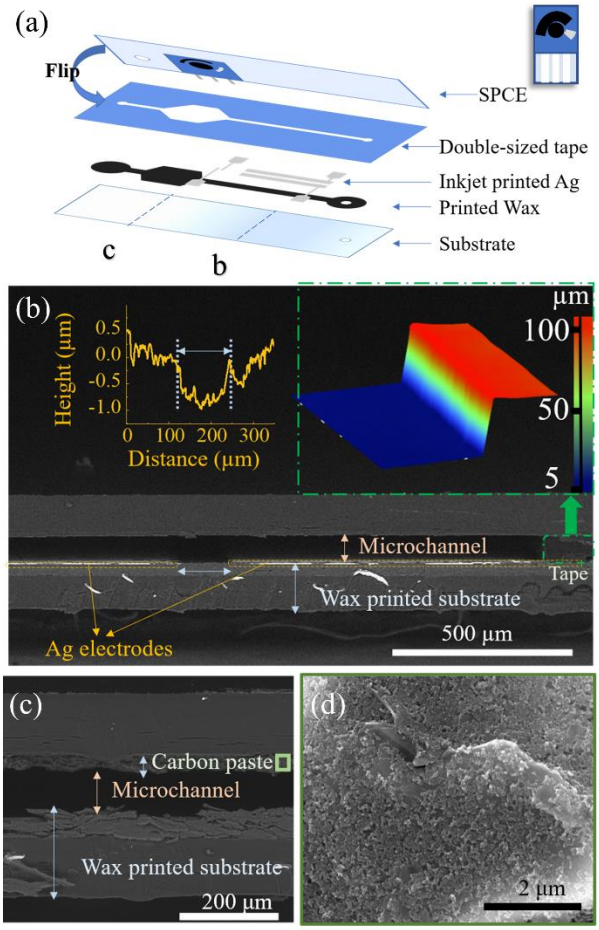

Figure 1. Scheme of the all-printed microfluidic sweat sensor (a), cross section of the microchannel, profilometry of the gap between two printed Ag electrodes (Inset left) and 3D profilometry of the open microchannel border (Inset right) (b), cross section of the HM chamber (c), and SEM picture of the SPCE working electrode (d).

3.2 Characterization of the HM microchamber and microchannel

The HM microchamber and microchannel were firstly investigated to verify the hollow structure was successfully created. The device cross-section along the microchannel (Figure 1(b)) was obtained by immersing it in liquid nitrogen and using a razor blade and a hammer to obtain a net cut and preserve the device structure. The cross section of the volume sensor showed clearly the channel, covered by the PET substrate of SPCE on top and the printed wax substrate at the bottom, with biadhesive tape blocking the

lateral side. The microchannel is about 80 μm in thickness, in partial accordance with the results of 3D profilometry (~99 μm). Besides, to know the thickness and the gap of the Ag electrodes, additional profilometry were performed, showing the electrodes thickness is approximately 600 nm with a gap width between the two electrodes of about 150 μm.

The HM microchamber was also characterized with the same method. In Figure 1(c), a stacked structure composed by the printed wax substrate, the microchamber, the SPCE, and its PET substrate is clearly observable. The height of the microchamber is the same of the microchannel (99 μm), which means the bulged SPCE (compared with the bare PET substrate) did not create any relevant deformation on the biadhesive tape. The morphology of the carbon paste electrode was also investigated (Figure 1(d)) showing the expected carbon flakes and particle structures, typical of this type of electrodes (Dong et al., 2007).

3.2 Sensing performance of the conductivity and of the volume nanosensors

The printed device was tested with NaCl solutions to define the sensing performance of both the conductivity and the volume AgNP nanosensors. For the conductivity nanosensor, the impedance changed from 100 kΩ (empty channel), to 30 kΩ when a 5 mM NaCl solution reached the electrodes. NaCl solutions with different concentrations were used to calibrate the conductivity nanosensor.

Figure 2(a), shows the staircase calibration results, with the impedance decreasing as the NaCl concentration increases. Figure 2(a) has been marked with different colors in connection with the cystic fibrosis cut-off sweat salts concentrations: green for concentrations associated with healthy condition, orange for dangerous concentrations requiring further investigation, and red for pathologic condition (NaCl concentration over 90 mM). (Lezana et al., 2003). The measured NaCl admittance resulted perfectly proportional with the NaCl concentration (Admittance $=2.95 \cdot 10^{-6} \times$Concentration$+1.17 \cdot 10^{-5}$, $R^2=0.99$), as shown in Figure 2(b).

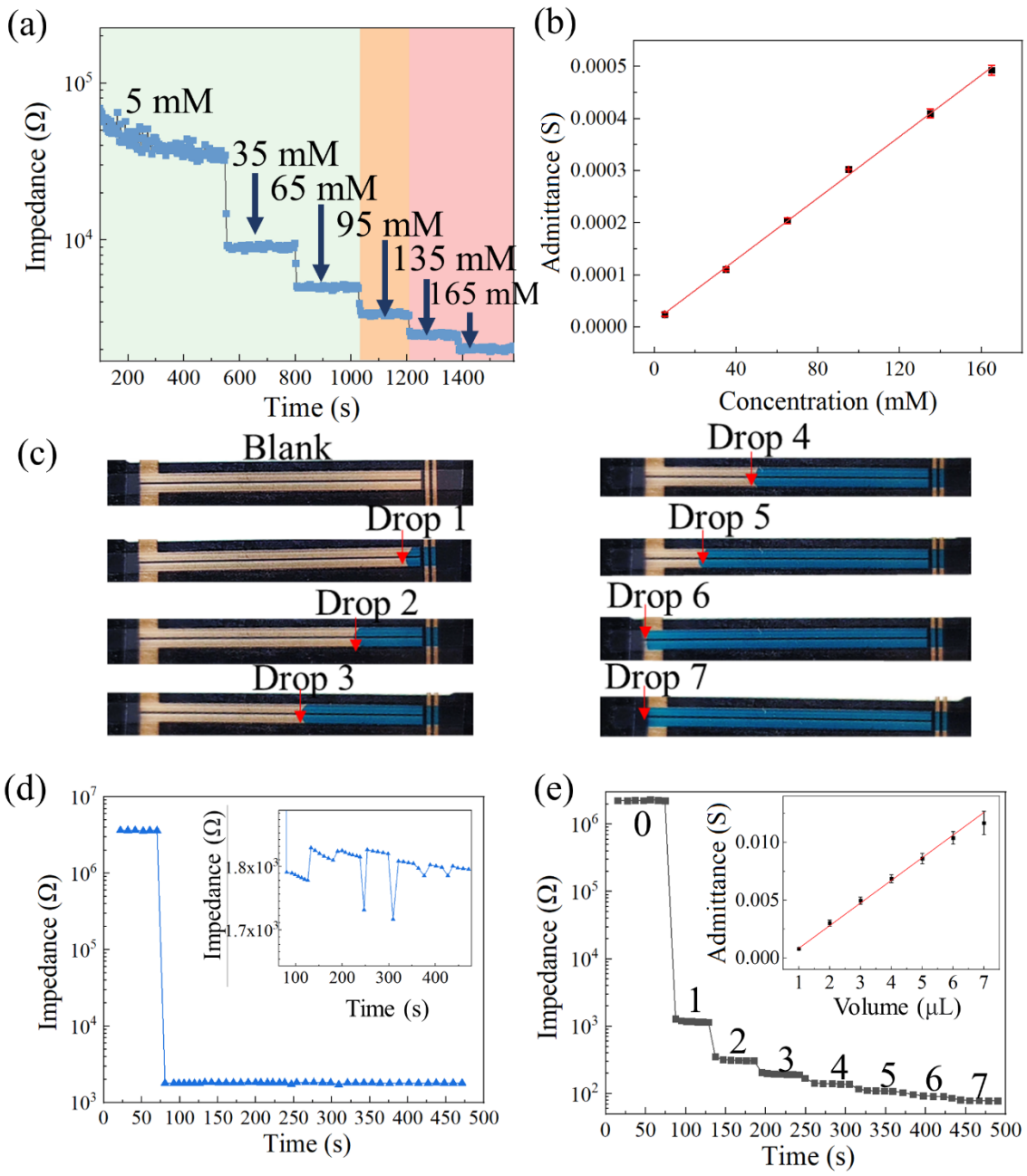

Figure 2. Staircase calibration of the conductivity nanosensor impedance with NaCl and CF diagnosis relevant ranges marked with colors (green=healthy, orange=suspicious, red=pathological) (a), admittance calibration curve (b), pictures of the microfluidic channel in correspondence to 1 µl colored dye drops at the device inlet (c), impedance of the conductivity sensor in correspondence to artificial sweat introduced drop-by-drop (d), impedance of the volume sensor with artificial sweat introduced drop-by-drop (e), and calibration of the volume nanosensor by means of its admittance (inset).

The volume nanosensor is printed along the microchannel. The more NaCl solution present in the microchannel, the more conduction takes place between the parallel electrodes, and thus, the less the impedance value. The empty microchannel impedance initial value (~$2 \cdot 10^6$ Ω) drops to less than 100 Ω when the channel is completely filled with artificial sweat.

The actual volume filling the channel can be easily inferred with any conductive solution from the volume nanosensor admittance thanks to the conductivity nanosensor admittance value. In fact, the volume nanosensor admittance (A_{volume}) is proportional to the volume by a constant (k) and the conductivity nanosensor admittance ($A_{conductivity}$) (Equation 1).

$$A_{volume} = k \cdot A_{conductivity} \cdot Volume \quad \text{(Eq. 1)}$$

The abovementioned equation has been experimentally verified with artificial sweat consecutive injections in the microchannel, for which the conductivity nanosensor impedance (admittance) remained constant after the initial drop (increase) when the solution reached the electrodes (Figure 2(d)), and the volume nanosensor impedance (admittance) decreased (increased) substantially at each injection (Figure 2(e)). The admittance calibration with respect to the injected volume ($A_{Volume} = 0.00169 \times Volume$, $R^2=0.99$) has allowed calculating the factor connecting the two nanosensor output values. Considering the normalization to the sweat admittance, k results equal to 3.042 μl^{-1}. Therefore, the volume of sweat can be calculated from the admittance measured by the two nanosensors as:

$$Volume = A_{volume} / (3.042 \cdot A_{conductivity}) \quad \text{(Eq. 2)}$$

3.3 Sensing performance of SPCEs in the microfluidic device

The SPCE in the printed microfluidic device was characterized with the $[Fe(CN)_6]^{4-}$/ $[Fe(CN)_6]^{3-}$ redox probe and Cu in artificial sweat using a commercial potentiostat. Figure 3(a) shows the cyclic voltammetry recorded in 5 mM $[Fe(CN)_6]^{4-}$/ $[Fe(CN)_6]^{3-}$ in 0.1 M KCl solution. Well-defined and quasi-reversible redox peaks were observed: the ratio between the anodic peak current (5.66 μA) and the cathodic one (-5.47μA) is almost the unit, in module. The oxidative and reductive peak potentials are 0.28

and -0.01 V, with a ΔE of 0.29 V, matching the results on SPCE reported in other works (Jian et al., 2013).

Artificial sweat spiked with Cu in the range between 500 and 2500 ppb was tested on the printed microfluidic device. The testing range was selected referring to a previous study reporting a healthy people range between 240 and 2400 ppb (Hohnadel et al., 1973).

The peak height of Cu showed a good correlation with the Cu concentration ($Ip=0.0023\cdot[Cu]-0.67$, $R^2=0.95$) in this range, as shown in Figure 3(b). The estimated limit of detection (LOD) and limit of quantification (LOQ) are 396 ppb and 1322 ppb, respectively. The LOD and LOQ were calculated as 3 and 10 times the standard deviation of the intercept over the slope of the calibration curve respectively., as reported in International Conference on Harmonization's (ICH) Q2 Validation of Analytical Procedures (Pérez-Ràfols et al., 2016).

The corresponding voltammograms in Figure 3(c) showed also a potential shift to positive potentials with increasing concentrations. This effect could be ascribed to the different deposition sites or surface morphology during the deposition of different amount of Cu (Ghanei-Motlagh et al., 2016; Hutton et al., 2011).

Once the calibration of the printed device was completed, a recovery test has been performed to test its accuracy. Artificial sweat spiked with 1500 ppb Cu was used to obtain the peak current value, which was then substituted into the calibration equation. The calculated concentration is 1675 ppb, with a recovery of 111.6% (Figure 3(d)). An interference test to prove the device selectivity towards other ions typically present in sweat (i.e., 120 ppb Mg^{2+}, 300 ppb Ni^{2+}, 0.5 ppb Cd^{2+}, 1300 ppb Zn^{2+}, 8000 ppb Ca^{2+}, 1600 ppb Fe^{3+}) (Bagheri et al., 2021) has been performed. With interference, the signal of 1400 ppb Cu is approximately 3.17 μA, to be compared to the 2.85 μA peak current of the one without interference, proving the interference can be considered negligible in our system (<10%) (Figure 3(e)).

Finally, to investigate the shelf life and the reproducibility of our system, a batch of devices were fabricated at day one and they were tested with 500 ppb Cu in artificial sweat every 2-4 days for a total of 23 days. The peak height fluctuated around 1.91 μA (RSD= 27%) (Figure 3(f)). However, after 23 days, due to the loss of hydrophilicity by the plasma treatment over time, the testing solution was unable to enter in the HM microchamber.

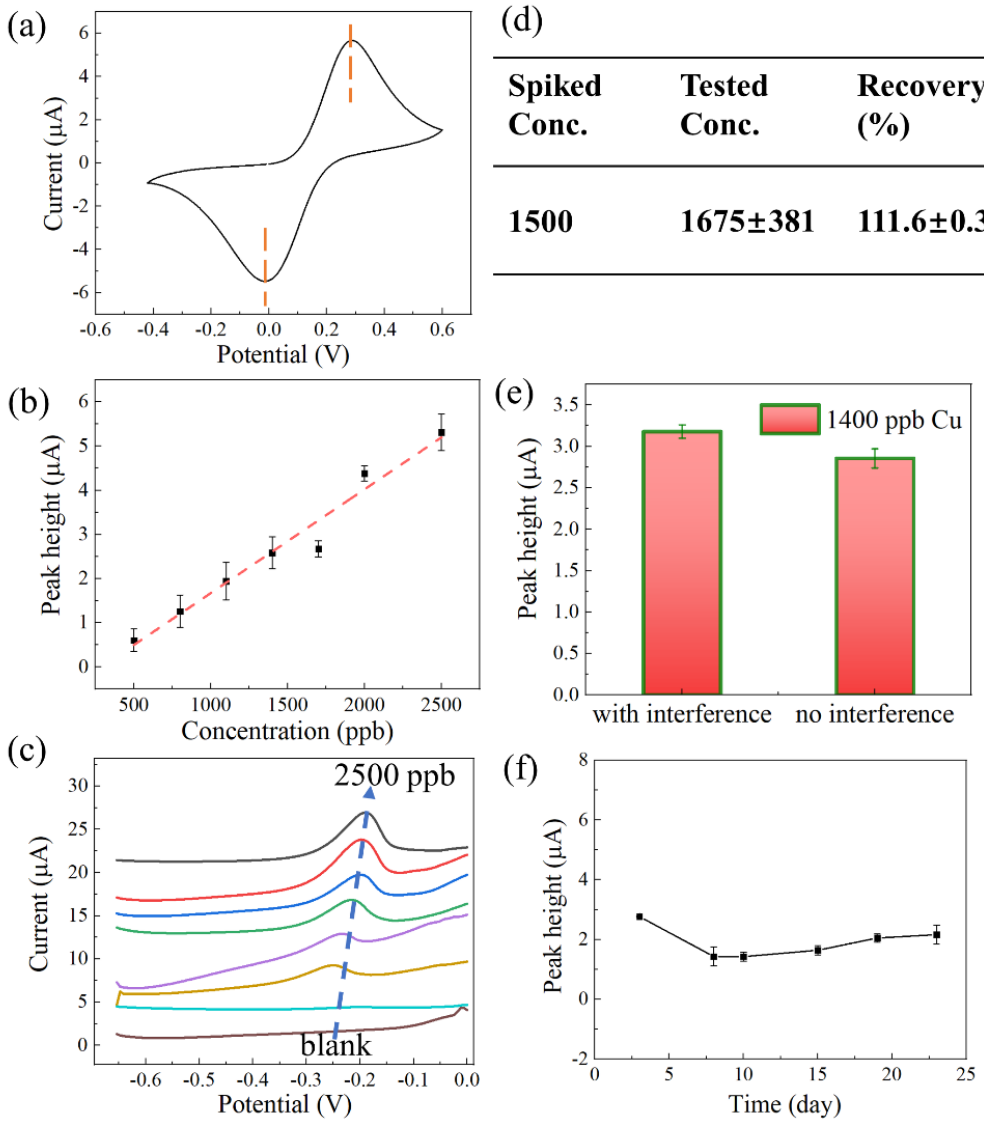

Spiked Conc.	Tested Conc.	Recovery (%)
1500	1675±381	111.6±0.3

Figure 3. Cyclic voltammetry of 5 mM $[Fe(CN)_6]^{4-}$/ $[Fe(CN)_6]^{3-}$ in 0.1 M KCl solution by SPCE in the printed device microchamber (a), calibration of Cu in artificial sweat by the SPCE in the microchamber (b), voltammograms from 0 to 2500 ppb Cu in artificial sweat by SPCE in the microchamber (c), recovery

test with 1500 ppb Cu (d), comparison of the peak currents with and without interference from other ions (e) 500 ppb Cu peak currents of sensors fabricated in the same batch from over time (f).

3.4 Wearable potentiostat

Wearable sensors will not have the practical use until they connect to a wearable potentiostat instead of bulky benchtop equipment. Hence, aiming for smaller size, less weight, and flexibility, we designed and fabricated a potentiostat on a flexible PCB board integrating all the components required for electrochemical measurements and wireless data transmission with mobile phones (Figure 4(a, b)). The system was built on a commercial electrochemical chip (LMP91000 chip), which is an integrated potentiostat to perform both two- and three-electrodes electrochemical measurements. The chip in our system is controlled by a programmable microcontroller, which is in turn connected to a low-power Bluetooth module for wireless communication with mobile phones. To achieve a friendlier user interface, a customized application based on Android system was developed, in which electrochemical measurements such as amperometry, cyclic voltammetry, and square wave voltammetry can be operated with the parameters set by users. Furthermore, the system has been designed to integrate a reverse iontophoresis module for active sweat sampling as proved in previous publications (Rao et al., 1995; Leboulanger et al., 2004, Girei et al., 2017), allowing to stimulate the perspiration anytime when a sample is needed. The whole platform also has a very low power consumption, which is supplied by a common 3V button battery.

For basic investigation of the flexible potentiostat, the artificial sweat with different concentrations of Cu were firstly tested by direct dropping on the SPCE surface, and the square wave voltammetry was operated with the flexible potentiostat controlled by the smartphone connected through Bluetooth. The set parameters were the same of the ones used with the commercial potentiostat (i.e., deposition time 200s, equilibrium time 20s, deposition potential –0.66 V, square-wave pulses with the frequency of 25 Hz, amplitude of 30 mV and potential step of 6 mV) except that the amplitude and potential step were 60 mV due to the limitation of the microelectrochemical chip ($\geqslant$ 60mV). The voltammograms in Figure 4(b),

showed an increasing peak with Cu concentration, from which a linear calibration can be defined (inset, Ip=0.081[Cu]+23.78, R^2=0.98). As a comparison, the printed microfluidic device was tested with three concentrations of Cu (500 ppb, 1400 ppb and 2500 ppb) in artificial sweat by the flexible potentiostat as shown in Figure 4(d). Compared with the direct drop method, the peak potential shifted in correspondence with lower Cu concentrations, due to the spatial limitation of the microchamber. Despite that, the printed microfluidic device was still able to distinguish the different concentration as low, mediate and high level (Figure 4 (d)).

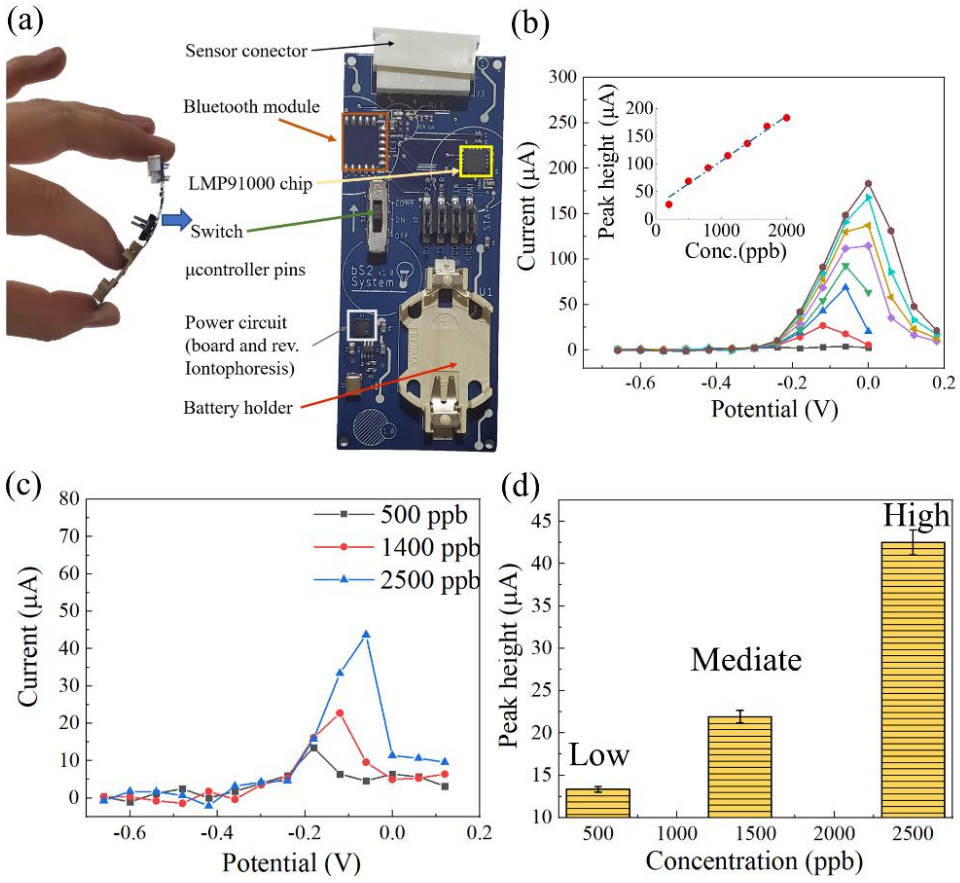

Figure 4. Picture of the flexible Bluetooth wearable potentiostat and schematic of the flexible PCB board, containing the integrated potentiostat (a), the validation of flexible potentiostat with mobile phone system by directly dropping artificial sweats on SPCE (b), the voltammograms of printed microfluidic device on the flexible potentiostat and mobile phone system (c), and the diagram of corresponding peak height.

To further explore the importance and novelty of this work, other recent sweat sensors for HM detection have been listed in Table 1. Generally, the electrodes in the reported works are composed of noble metal (e.g., Au) fabricated with cleanroom facilities and methods. Additionally, the reported sensing systems lacks a microfluidic system to monitor the sweat rate and volume. Moreover, the corresponding measuring systems are based on commercial bulky potentiostat. Conversely, in this study, simple printing techniques were used to fabricate a microfluidic device to detect Cu and measure the conductivity and the volume of sweat samples, which can be obtained thanks to the reverse iontophoresis function of our wearable potentiostat. Finally, our system can be used in conjunction with a customized flexible wearable integrated low-power.

Despite our higher LOD and lower sensitivity, which may be attributed to the bare carbon paste with limited affinity to Cu, we are operating in the clinical concentration of Cu in sweat, normally in the 240-2400 ppb range.

Table 1. Comparison with other heavy metal sweat sensors.

	Analytes	LOD (ppb)	Sensitivity (nA/ppb)	Calibration range	Electrode	Fabrication techniques	Sweat volume	REF
1	Zn, Cd, Pb, Cu, and Hg	-	4.1	0 - 300 ppb	Au and Bi with Nafion	Photolithography	No	(Gao et al., 2016)
2	Cu, Zn	0.1	-	300–1500 ppb	Au modified $Ti_3C_2T_x$ and MWNTs	Photolithography	No	(Park et al., 2020)

3	Cu	3	10.7	10-400 ppb	AuNPs modified Carbon	Printing techniques	No	(Bagheri et al., 2021)
4	Zn	-	-	0-2000 ppb	Au on glove	Shadow mask sputtering	No	(Bariya et al., 2020)
5	Zn	50	23.8	100 -2000 ppb	Bismuth on Nafion and Carbon	Electroplating on printed Carbon electrode	No	(Kim et al., 2015)
6	Na	-	-	15-120 mM	Au	Photolithography	Yes	(Nyein et al., 2018)
7	Cu	396	2.3	500-2500 ppb	Carbon paste	Screen printing	Yes	This study
8	Na	-	-	5-165 mM	AgNPs	Inkjet printing	Yes	

4. Conclusions

In this work, we have proved that a fully-printed wearable biosensor for the detection and quantification of copper excreted in sweat is feasible. Furthermore, we integrated in our wearable system an active perspiration stimulating device based on reverse iontophoresis, a simple sweat rate normalization device, and a flexible miniaturized wireless potentiostat managed by a custom smartphone app. With our simplified solution, we have managed to address many of the common issues in sensor development such as sample extraction, sweat rate normalization, real-time measurements, and continuous monitoring. All the components of our system have been validated in the lab using spiked artificial sweat and optimizing the fabrication and measuring parameters of each component. Despite our relatively high LOD with respect to other Cu sweat sensors (Table 1), we fit in the clinical range of interest, and our system makes

use only of printed low-cost and flexible solutions. The interference resilience and shelf life of our system makes it an interesting choice for practical applications and continuous monitoring.

Acknowledgments

This publication is part of the I+D+i Projects MAT2017-87202-P and SEV2201320295, funded by MCIN/ AEI/10.13039/501100011033/. ICN2 is funded by the CERCA Program/Generalitat de Catalunya.

Qiuyue Yang acknowledge the support and funding by Chinese Scholarship Council.

Vernalyn Abarintos acknowledge the support and funding by the Department of Science and Technology - Science Education Institute.

Miguel Angel Aroca acknowledge the support and funding by the Gobernación del Cesar through resources of Science, Technology, and Innovation for the higher education of the Ministry of Science, Technology, and Innovation under grant 681-2014.

We acknowledge the work of David Ricard Fort (Universidad Polytecnica de Catalunya) during his internship in the NBB ICN2 group, developing conductive hydrogels for reverse iontophoresis and impermeabilization methods for the absorbent substrate used for the printed sensors.

References

Agarwal, A., Avarebeel, S., Choudhary, N.S., Goudar, M., Tejaswini, C.., 2017. Correlation of Trace Elements in Patients of Chronic Liver Disease with Respect to Child- Turcotte- Pugh Scoring System. J. Clin. Diagn. Res. 11, OC25. https://doi.org/10.7860/JCDR/2017/26519.10655

Anastasova, S., Crewther, B., Bembnowicz, P., Curto, V., Ip, H.M., Rosa, B., Yang, G.Z., 2017. A wearable multisensing patch for continuous sweat monitoring. Biosens. Bioelectron. 93, 139–145. https://doi.org/10.1016/J.BIOS.2016.09.038

Aruoma, O.I., Reilly, T., MacLaren, D., Halliwell, B., 1988. Iron, copper and zinc concentrations in human sweat and plasma; the effect of exercise. Clin. Chim. Acta 177, 81–87. https://doi.org/10.1016/0009-8981(88)90310-5

B, L., RH, G., MB, D.-C., 2004. Reverse iontophoresis for non-invasive transdermal monitoring. Physiol. Meas. 25. https://doi.org/10.1088/0967-3334/25/3/R01

Bagheri, N., Mazzaracchio, V., Cinti, S., Colozza, N., Natale, C. Di, Netti, P.A., Saraji, M., Roggero, S., Moscone, D., Arduini, F., 2021. Electroanalytical Sensor Based on Gold-Nanoparticle-Decorated

Paper for Sensitive Detection of Copper Ions in Sweat and Serum. Anal. Chem. 93, 5225–5233. https://doi.org/10.1021/acs.analchem.0c05469

Bandodkar, A.J., Jeang, W.J., Ghaffari, R., Rogers, J.A., 2019. Wearable Sensors for Biochemical Sweat Analysis. Annu. Rev. ofAnalytical Chem. 12, 1–22. https://doi.org/10.1146/ANNUREV-ANCHEM-061318-114910

Bariya, M., Li, L., Ghattamaneni, R., Ahn, C.H., Nyein, H.Y.Y., Tai, L.C., Javey, A., 2020. Glove-based sensors for multimodal monitoring of natural sweat. Sci. Adv. 6, 1–10. https://doi.org/10.1126/sciadv.abb8308

Bariya, M., Nyein, H.Y.Y., Javey, A., 2018. Wearable sweat sensors. Nat. Electron. 2018 13 1, 160–171. https://doi.org/10.1038/s41928-018-0043-y

Brothers, M.C., DeBrosse, M., Grigsby, C.C., Naik, R.R., Hussain, S.M., Heikenfeld, J., Kim, S.S., 2019. Achievements and Challenges for Real-Time Sensing of Analytes in Sweat within Wearable Platforms. Acc. Chem. Res. 52, 297–306. https://doi.org/10.1021/ACS.ACCOUNTS.8B00555

Chung, M., Fortunato, G., Radacsi, N., 2019. Wearable flexible sweat sensors for healthcare monitoring: a review. J. R. Soc. Interface 16, 1–15. https://doi.org/10.1098/RSIF.2019.0217

Dong, H., Li, C.-M., Zhang, Y.-F., Cao, X.-D., Gan, Y., 2007. Screen-printed microfluidic device for electrochemical immunoassay. Lab Chip 7, 1752–1758. https://doi.org/10.1039/B712394A

Gao, W., Nyein, H.Y.Y., Shahpar, Z., Fahad, H.M., Chen, K., Emaminejad, S., Gao, Y., Tai, L.C., Ota, H., Wu, E., Bullock, J., Zeng, Y., Lien, D.H., Javey, A., 2016. Wearable Microsensor Array for Multiplexed Heavy Metal Monitoring of Body Fluids. ACS Sensors 1, 866–874. https://doi.org/10.1021/acssensors.6b00287

Ghaffari, R., Rogers, J.A., Ray, T.R., 2021. Recent progress, challenges, and opportunities for wearable biochemical sensors for sweat analysis. Sensors Actuators B Chem. 332, 129447. https://doi.org/10.1016/J.SNB.2021.129447

Ghanei-Motlagh, M., Karami, C., Taher, M.A., Hosseini-Nasab, S.J., 2016. Stripping voltammetric detection of copper ions using carbon paste electrode modified with aza-crown ether capped gold nanoparticles and reduced graphene oxide. RSC Adv. 6, 89167–89175. https://doi.org/10.1039/C6RA10267K

Giri, T.K., Chakrabarty, S., Ghosh, B., 2017. Transdermal reverse iontophoresis: A novel technique for therapeutic drug monitoring. J. Control. Release 246, 30–38. https://doi.org/10.1016/J.JCONREL.2016.12.007

Gutteridge, J.M.C., Rowley, D.A., Halliwell, B., Cooper, D.F., Heeley, D.M., 1985. Copper and iron complexes catalytic for oxygen radical reactions in sweat from human athletes. Clin. Chim. Acta 145, 267–273. https://doi.org/10.1016/0009-8981(85)90033-6

Hohnadel, D.C., Sunderman Jr., F.W., Nechay, M.W., McNeely, M.D., 1973. Atomic Absorption Spectrometry of Nickel, Copper, Zinc, and Lead in Sweat Collected from Healthy Subjects during Sauna Bathing. Clin. Chem. 19, 1288–1292. https://doi.org/10.1093/clinchem/19.11.1288

Hutton, L.A., Newton, M.E., Unwin, P.R., Macpherson, J. V, 2011. Factors Controlling Stripping Voltammetry of Lead at Polycrystalline Boron Doped Diamond Electrodes: New Insights from High-Resolution Microscopy. Anal. Chem. 83, 735–745. https://doi.org/10.1021/ac101626s

Jian, J.-M., Liu, Y.-Y., Zhang, Y.-L., Guo, X.-S., Cai, Q., 2013. Fast and Sensitive Detection of Pb2+ in Foods Using Disposable Screen-Printed Electrode Modified by Reduced Graphene Oxide. Sensors . https://doi.org/10.3390/s131013063

Jo, S., Sung, D., Kim, S., Koo, J., 2021. A review of wearable biosensors for sweat analysis. Biomed. Eng. Lett. 2021 11, 117–129. https://doi.org/10.1007/S13534-021-00191-Y

Kim, J., Campbell, A.S., de Ávila, B.E.-F., Wang, J., 2019. Wearable biosensors for healthcare monitoring. Nat. Biotechnol. 37, 389–406. https://doi.org/10.1038/s41587-019-0045-y

Kim, J., De Araujo, W.R., Samek, I.A., Bandodkar, A.J., Jia, W., Brunetti, B., Paixão, T.R.L.C., Wang, J., 2015. Wearable temporary tattoo sensor for real-time trace metal monitoring in human sweat. Electrochem. commun. 51, 41–45. https://doi.org/10.1016/j.elecom.2014.11.024

Klevay, L.M., 1975. Coronary heart disease: the zinc/copper hypothesis. Am. J. Clin. Nutr. 28, 764–774. https://doi.org/10.1093/AJCN/28.7.764

Lee, H.B., Meeseepong, M., Trung, T.Q., Kim, B.Y., Lee, N.E., 2020. A wearable lab-on-a-patch platform with stretchable nanostructured biosensor for non-invasive immunodetection of biomarker in sweat. Biosens. Bioelectron. 156, 112133. https://doi.org/10.1016/J.BIOS.2020.112133

Lezana, J.L., Vargas, M.H., Karam-Bechara, J., Aldana, R.S., Furuya, M.E.Y., 2003. Sweat conductivity and chloride titration for cystic fibrosis diagnosis in 3834 subjects. J. Cyst. Fibros. 2, 1–7. https://doi.org/https://doi.org/10.1016/S1569-1993(02)00146-7

Liu, C., Xu, T., Wang, D., Zhang, X., 2020. The role of sampling in wearable sweat sensors. Talanta 212, 120801. https://doi.org/10.1016/J.TALANTA.2020.120801

Mohan, A.M.V., Rajendran, V., Mishra, R.K., Jayaraman, M., 2020. Recent advances and perspectives in sweat based wearable electrochemical sensors. TrAC Trends Anal. Chem. 131, 116024. https://doi.org/10.1016/J.TRAC.2020.116024

Montain, S.J., Cheuvront, S.N., Lukaski, H.C., 2007. Sweat Mineral-Element Responses during 7 h of Exercise-Heat Stress. Int. J. Sport Nutr. Exerc. Metab. 17, 574–582. https://doi.org/10.1123/IJSNEM.17.6.574

Morales-Narvaez, E., Dincer, C., 2021. Wearable physical, chemical and biological sensors : fundamentals, materials and applications.

Nangliya, V., Sharma, A., Yadav, D., Sunder, S., Nijhawan, S., Mishra, S., 2015. Study of Trace Elements in Liver Cirrhosis Patients and Their Role in Prognosis of Disease. Biol. Trace Elem. Res. 165, 35–40. https://doi.org/10.1007/S12011-015-0237-3

Nyein, H.Y.Y., Tai, L.-C., Ngo, Q.P., Chao, M., Zhang, G.B., Gao, W., Bariya, M., Bullock, J., Kim, H., Fahad, H.M., Javey, A., 2018. A Wearable Microfluidic Sensing Patch for Dynamic Sweat Secretion Analysis. ACS Sensors 3, 944–952. https://doi.org/10.1021/ACSSENSORS.7B00961

Park, J.Y., Hui, X., Sharifuzzaman, M., Sharma, S., Xuan, X., Zhang, S., Ko, S.G., Yoon, S.H., 2020. High-performance flexible electrochemical heavy metal sensor based on layer-by-layer assembly of Ti3C2Tx/MWNTs nanocomposites for noninvasive detection of copper and zinc ions in human biofluids. ACS Appl. Mater. Interfaces 12, 48928–48937. https://doi.org/10.1021/acsami.0c12239

Pérez-Ràfols, C., Serrano, N., Díaz-Cruz, J.M., Ariño, C., Esteban, M., 2016. Glutathione modified screen-printed carbon nanofiber electrode for the voltammetric determination of metal ions in natural samples. Talanta 155, 8–13. https://doi.org/https://doi.org/10.1016/j.talanta.2016.04.011

Qiao, L., Benzigar, M.R., Subramony, J.A., Lovell, N.H., Liu, G., 2020. Advances in Sweat Wearables: Sample Extraction, Real-Time Biosensing, and Flexible Platforms. ACS Appl. Mater. Interfaces 12, 34337–34361. https://doi.org/10.1021/ACSAMI.0C07614

Rao, G., Guy, R.H., Glikfeld, P., LaCourse, W.R., Leung, L., Tamada, J., Potts, R.O., Azimi, N., 1995. Reverse Iontophoresis: Noninvasive Glucose Monitoring in Vivo in Humans. Pharm. Res. 12, 1869–1873. https://doi.org/10.1023/A:1016271301814

Rosati, G. Urban, M., Zhao, L., Yang, Q., Silva, C.C.C., Bonaldo, S., Parolo, C., Nguyen, E.P., Ortega, G., Fornasiero, P, Paccagnella, A., Merkoçi, A. A Plug, Print & Play inkjet printing and impedance-based biosensing technology operating through a smartphone for clinical diagnostics. Biosensors and Bioelectronics (accepted for publication)

Salvo, P., Di Francesco, F., Costanzo, D., Ferrari, C., Trivella, M.G., De Rossi, D., 2010. A wearable sensor for measuring sweat rate. IEEE Sens. J. 10, 1557–1558. https://doi.org/10.1109/JSEN.2010.2046634

Saraymen, R., Kılıç, E., Yazar, S., Güreşçilerde, M., Çinko, T., Seviyeleri, K., 2004. Sweat Copper, Zinc, Iron, Magnesium and Chromium Levels in National Wrestler. İnönü Üniversitesi Tıp Fakültesi Derg. 11, 7–10.

Saraymen, R., Kılıç, E., Yazar, S., Saraymen, B., 2003. Magnesium, Copper, Zinc, Iron, and Chromium Levels in Sweat of Boxers. İnönü Üniversitesi Tıp Fakültesi Derg. 10, 121–125.

Schaefer, M., Schellenberg, M., Merle, U., Weiss, K.H., Stremmel, W., 2008. Wilson protein expression, copper excretion and sweat production in sweat glands of Wilson disease patients and controls. BMC Gastroenterol. 8, 1–9. https://doi.org/10.1186/1471-230X-8-29

Silva, R.R., Raymundo-Pereira, P.A., Campos, A.M., Wilson, D., Otoni, C.G., Barud, H.S., Costa, C.A.R., Domeneguetti, R.R., Balogh, D.T., Ribeiro, S.J.L., Oliveira, O.N., 2020. Microbial nanocellulose adherent to human skin used in electrochemical sensors to detect metal ions and biomarkers in sweat. Talanta 218. https://doi.org/10.1016/j.talanta.2020.121153

Silva, R.R., Raymundo-Pereira, P.A., Campos, A.M., Wilson, D., Otoni, C.G., Barud, H.S., Costa, C.A.R., Domeneguetti, R.R., Balogh, D.T., Ribeiro, S.J.L., Oliveira, O.N., 2020. Microbial nanocellulose adherent to human skin used in electrochemical sensors to detect metal ions and biomarkers in sweat. Talanta 218. https://doi.org/10.1016/j.talanta.2020.121153

Siquier-Coll, J., Bartolomé, I., Perez-Quintero, M., Grijota, F.J., Muñoz, D., Maynar-Mariño, M., 2020. Effects of exposure to high temperatures on serum, urine and sweat concentrations of iron and copper. J. Therm. Biol. 89, 102536. https://doi.org/10.1016/J.JTHERBIO.2020.102536

Souza, A.P.R.D., Lima, A.S., Salles, M.O., Nascimento, A.N., Bertotti, M., 2010. The use of a gold disc microelectrode for the determination of copper in human sweat. Talanta 83, 167–170. https://doi.org/10.1016/J.TALANTA.2010.09.001

Stauber, J.L., Florence, T.M., 1987. The determination of trace metals in sweat by anodic stripping voltammetry. Sci. Total Environ. 60, 263–271. https://doi.org/10.1016/0048-9697(87)90420-7

Sunderman, F.W., Hohnadel, D.C., Evenson, M.A., Wannamaker, B.B., Dahl, D.S., 1974. Excretion o f Copper in Sweat o f Patients with Wilson's Disease During Sauna Bathing. Ann. Clin. Lab. Sci. 4, 407–412.

Tomasz Saran, T., Magdalena Zawadka, M., Stanisław Chmiel, S., Anna Mazur, A., 2018. Sweat lead and copper concentrations during exercise training. Eur. J. Clin. Exp. Med. 16, 14–19. https://doi.org/10.15584/EJCEM.2018.1.2

Vaquer, A., Barón, E., Rica, R. de la, 2020. Wearable Analytical Platform with Enzyme-Modulated Dynamic Range for the Simultaneous Colorimetric Detection of Sweat Volume and Sweat Biomarkers. ACS Sensors 6, 130–136. https://doi.org/10.1021/ACSSENSORS.0C01980

Vierling, J.M., 2008. Copper Metabolism in Primary Biliary Cirrhosis. Semin. Liver Dis. 1, 293–308. https://doi.org/10.1055/S-2008-1040733

Vinoth, R., Nakagawa, T., Mathiyarasu, J., Mohan, A.M.V., 2021. Fully Printed Wearable Microfluidic Devices for High-Throughput Sweat Sampling and Multiplexed Electrochemical Analysis. ACS Sensors 6, 1174–1186. https://doi.org/10.1021/ACSSENSORS.0C02446

Xu, J., Fang, Y., Chen, J., 2021. Wearable Biosensors for Non-Invasive Sweat Diagnostics. Biosensors 11, 245. https://doi.org/10.3390/BIOS11080245

Yang, Q., Nagar, B., Alvarez-Diduk, R., Balsells, M., Farinelli, A., Bloisi, D., Proia, L., Espinosa, C., Ordeix, M., Knutz, T., De Vito-Francesco, E., Allabashi, R., Merkoçi, A., 2021. Development of a Heavy Metal Sensing Boat for Automatic Analysis in Natural Waters Utilizing Anodic Stripping Voltammetry. ACS ES&T Water. https://doi.org/10.1021/acsestwater.1c00192

Yetisen, A.K., Martinez-Hurtado, J.L., Ünal, B., Khademhosseini, A., Butt, H., 2018. Wearables in Medicine. Adv. Mater. 30, 1706910. https://doi.org/10.1002/ADMA.201706910

Youssef, A.A., Wood, B., Baron, D.N., 1983. Serum copper: a marker of disease activity in rheumatoid arthritis. J. Clin. Pathol. 36, 14–17. https://doi.org/10.1136/JCP.36.1.14

Zhong Zhang, Morteza Azizi, Michelle Lee, Philip Davidowsky, Peter Lawrence, Alireza Abbaspourrad, 2019. A versatile, cost-effective, and flexible wearable biosensor for in situ and ex situ sweat analysis, and personalized nutrition assessment. Lab Chip 19, 3448–3460. https://doi.org/10.1039/C9LC00734B